

Generalisable 3D Fabric Architecture for Streamlined Universal Multi-Dataset Medical Image Segmentation

Siyu Liu¹, Wei Dai¹, Craig Engstrom¹, Jurgen Fripp², Stuart Crozier¹, Jason A. Dowling², Shekhar S. Chandra¹

¹School of Information Technology and Electrical Engineering, University of Queensland, Australia

²Australian e-Health Research Centre, CSIRO, Australia

Abstract—Data scarcity is common in deep learning models for medical image segmentation. Previous works proposed multi-dataset learning, either simultaneously or via transfer learning to expand training sets. However, medical image datasets have diverse-sized images and features, and developing a model simultaneously for multiple datasets is challenging. This work proposes Fabric Image Representation Encoding Network (FIRENet), a universal 3D architecture for simultaneous multi-dataset segmentation and transfer learning involving arbitrary numbers of dataset(s). To handle different-sized image and feature, a 3D fabric module is used to encapsulate many multi-scale sub-architectures. An optimal combination of these sub-architectures can be implicitly learnt to best suit the target dataset(s). For diverse-scale feature extraction, a 3D extension of atrous spatial pyramid pooling (ASPP3D) is used in each fabric node for a fine-grained coverage of rich-scale image features. In the first experiment, FIRENet performed 3D universal bone segmentation of multiple musculoskeletal datasets of the human knee, shoulder and hip joints and exhibited excellent simultaneous multi-dataset segmentation performance. When tested for transfer learning, FIRENet further exhibited excellent single dataset performance (when pre-training on a prostate dataset), as well as significantly improved universal bone segmentation performance. The following experiment involves the simultaneous segmentation of the 10 Medical Segmentation Decathlon (MSD) challenge datasets. FIRENet demonstrated good multi-dataset segmentation results and inter-dataset adaptability of highly diverse image sizes. In both experiments, FIRENet’s streamlined multi-dataset learning with one unified network that requires no hyper-parameter tuning.

Deep learning for medical image segmentation is a rapidly evolving field with the potential to enhance disease diagnosis [36] and treatment planning [43]. The effectiveness of deep learning can be largely attributed to its data-driven nature. However, this reliance on data is also a major limitation in medical image segmentation due to data scarcity. Unlike the abundance of large-scale public datasets [34], [18], [9] in 2D computer-vision tasks, (expert) labelled medical image datasets are much smaller in quantity due to several factors:

- Data acquisition challenges: The acquisition of medical images can be highly specialised and resource-intensive. Voxel-wise manual annotation of 3D volumes (for segmentation) is time-intensive and subject to variable operator error. In addition, careful planning and expert contouring protocols are usually required to minimise intra- and inter-rater segmentation variability.
- Data fragmentation: Clinical studies involving medical imaging are typically highly focused, relatively small

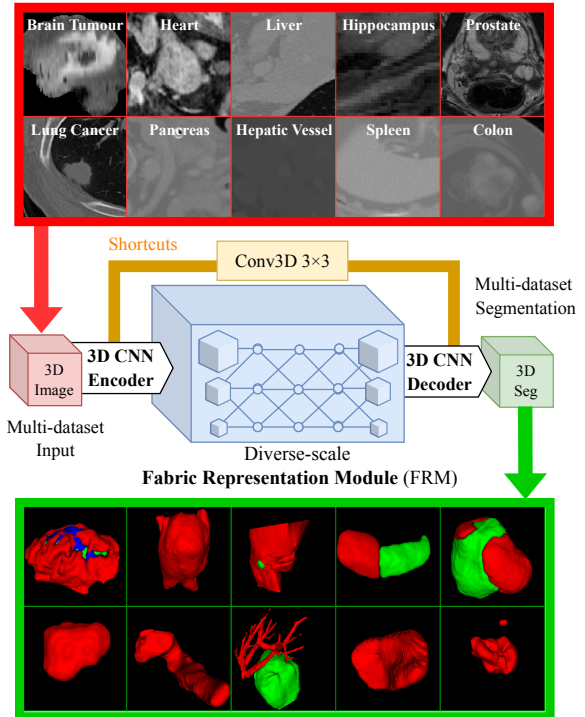


Fig. 1: Simultaneous 3D segmentation of the 10 Medical Segmentation Decathlon (MSD) challenge datasets using only one instance of Fabric Image Representation Encoding Network (FIRENet). FIRENet uses a the latent fabric module to process diverse-sized features and images.

investigations due to high imaging costs. Datasets from different studies can exhibit considerable inter-dataset variations (for example, different imaging fields of view, and dimensions) associated with different acquisition sequences and protocols. Most models lack versatility as they are highly optimised for only one dataset at a time.

- Access to imaging datasets: Collecting large-scale medical image datasets with expert annotations is difficult as explicit consent, strict adherence to ethics and systematic coordination are required, as the publication of patient data, even when de-identified, is a highly sensitive matter.

When facing data scarcity, multi-dataset applications including transfer learning [52], [7] and simultaneous multi-dataset

learning [23]) have been shown to improve segmentation performance. However, most current deep learning methods for medical image analysis are designed for application on very few datasets. Even architectures that can adapt to different datasets, like nnUNet [25], are optimised for one dataset at a time. Works that use one model to aggregate from and transfer features to many datasets remain limited. Currently, existing (and notable) works for simultaneous multi-dataset segmentation in the literature are 3D MDUNet and 3DU²Net, which applied a U-Net-like architecture simultaneously to several MSD challenge datasets. However, they only demonstrated limited applicability on a subset of the available MSD datasets. To extend the coverage to more datasets with diverse features and sizes, a model with more focus on diverse-scale feature extraction and architecture-level versatility is desirable.

Fabric-based architectures [57], [19], [42] are an ideal candidate for multi-dataset processing as they create a superposition of many multi-scale sub-architectures. With this inspiration, this work proposes FIRENet, a versatile 3D network that leverages a convolutional fabric for multi-dataset medical image segmentation. The central features of FIRENet are:

- 1) For improved adaptation to different medical image datasets, FIRENet’s uses a 3D fabric representation module (FRM) to emulate a superposition of many multi-scale sub-architectures. The major advantage of FRM is architecture-level generalisability, which is essential as different datasets contain different image and feature sizes.
- 2) To harness the benefits of multi-scale feature extraction for processing diverse features, FRM consists of multi-scale branches of fabric nodes. Furthermore, a 3D extension of atrous spatial pyramid pooling (ASPP) [5] is employed in each FRM node to provide fine-grained coverage of different-sized features.
- 3) The nodes in FRM are connected via trainable feature sum (TFS) to further optimise FIRENet’s multi-dataset adaptability. These connections can be trained to automatically form an architecture from different medical image datasets. (Figure 1).
- 4) FIRENet’s generalisable architecture ensures no hyper-parameter modification is required when applying or transferring it to multiple datasets.

FIRENet’s demonstrated good performance and versatility in various transfer learning and multi-dataset segmentation tasks. The transfer learning and simultaneous multi-dataset segmentation experiments show FIRENet’s versatility in various medical image segmentation tasks, including I) standard single dataset segmentation (during pre-training on an MR prostate dataset) II) simultaneous universal (support for multi-anatomy) bone segmentation with and without transfer learning, and III) simultaneous multi-object segmentation performance for all the 10 image datasets in the MSD challenge. Notably, FIRENet also exhibits multi-dataset adaptability without tailored training procedures to reach

convergence.

I. RELATED WORK

A. Convolutional Neural Networks (CNNs) for image segmentation

The most common class of deep learning models for (medical) image segmentation are CNNs. CNNs were initially developed for image classification [29], [45] and were later found suitable for image segmentation tasks. Typically, CNNs use consecutive convolution (image filtering) and hierarchical down-sampling to task-related extract features. However, since image segmentation require dense (pixel or voxel-wise) predictions, image segmentation models require feature learning at both global (coarse) and local (fine-detailed) scales. Excessive down-sampling, as used in classic CNNs [45], [22] can degrade segmentation accuracy due to loss of image resolution. In response, later works, including UNet [41], incorporated an encoder-decoder architecture that first extracts large-context features using an encoder CNN, then re-constructs the full-resolution image using a decoder CNN (reversing the down-sampling performed by the encoder). To further aid the decoder in recovering fine details, UNet also makes use of shortcuts for passing high-resolution features directly from the encoder to the decoder. There have been several recent UNet-based networks [58], [55], [39], [59] successfully applied to medical image segmentation tasks.

B. CNNs for improved architecture generalisability

Most early-day CNNs were only suitable for processing limited image and feature sizes, which is not ideal for models intended for complex features or in this case, multiple datasets. In response, multi-scale feature extraction [17], [38], [2], [56], [31] was introduced and has become a common inclusion in CNNs for extracting diverse-sized features. Typically, multi-scale feature extraction divides the input into several parallel branches, each with a different receptive field size. For example, the atrous spatial pyramid pooling (ASPP) in DeepLabV3 [5], [6] uses several parallel dilated [53] convolution layers to achieve multi-scale feature extraction. Another more recent multi-scale network achieving state-of-the-art 2D image segmentation performance is the HRNet [48], which also frequently exchanges multi-scale features extracted through parallel branches. From another perspective, multi-scale networks like DeepLabV3 and HRNet are in essence, ensembles of many sub-architectures allowing multi-scaled features to be aggregated. Through training, the network can decide the optimal combination of features that best suit the data.

In pursuit of more explicit architecture-level adaptation to arbitrary datasets, works such as nnUNet [25] introduced a procedural method to self-configure models according to the geometry of the training dataset. The result is a highly-curated model that suits different training datasets, albeit one at a time. In the meantime, there have also been gradient-based self-configuring networks. Fabric-like CNNs [57], [19], [42] were proposed to encapsulate many sub-architectures using interlaced multi-scale convolutional

blocks, and all the blocks are trained end-to-end using gradient descent. Recently, Neural Architecture Search (NAS) methods like AutoDeepLab [35], [54], [60] have demonstrated more explicit gradient-based self-configuration. It employed weighted trainable connections between cells during training. During training, these weights are tuned to best adapt to the training data. After training, weak connections can be pruned to reveal a compact architecture for the specific training set. The resulting architecture was found to be as successful as many hand-crafted architectures. However, for multi-dataset training, the limitation of these methods is that they are highly curated, and thus the resulting models are not generally applicable to diverse datasets.

1) *Simultaneous multi-dataset 3D medical image segmentation*: Since most segmentation techniques are transferable between 2D and 3D, 3D medical image segmentation methods have been rapidly evolving by building on works in both 2D and 3D. Some 2D works were first transferred to 3D without major modification [8], [37]. Over time, 3D segmentation methods have become increasingly sophisticated [21], [32], [46], [47]. However, 3D medical image segmentation still needs to combat data scarcity and memory consumption issues.

Incorporating multiple datasets when training a segmentation model can be a solution to data scarcity. Multi-dataset works such as transfer learning [40], [28], [49], [44], [7] and simultaneous multi-dataset learning [23], [50], [24], [33] have demonstrated weight-sharing as a practical way to improve performance. However, these methods are limited to a small number of datasets. For example, [50] uses components developed for a limited scope (CT lesion detection). While [23], [33] and [24] demonstrated more flexibility by incorporating domain adapters, they only demonstrated simultaneous segmentation on a small subset of the available datasets (in the MSD challenge). Currently, only a small number of works have achieved large-scale applicability to different datasets.

Memory consumption is bound to affect 3D CNNs when applied simultaneously to diverse-sized datasets. In the literature, workarounds such as reducing model complexity [8] are often required to train 3D CNNs. However, overly simplifying a CNN architecture can limit its multi-dataset learning capacity. Alternatively, patch-based methods [10], [12], [14], [13] are often used to divide the large 3D volume into smaller patches. However, this also results in additional hyper-parameters such as patch size, which are dataset-specific. Hence, for simultaneous multi-dataset 3D segmentation, it is important to ensure the model is as end-to-end as possible.

II. METHODS

A. Network architecture

1) *Encoder decoder structure*: FIRENet is a 3D CNN encoder-decoder with a fabric representation module (FRM) (Figure 2 top block) in the bottleneck. The encoder performs progressive down-sampling on the input while widening the depth using two residual blocks of 32 and 64 filters, and the decoder mirrors the encoder structure to recover image resolution. UNet-like shortcuts are used to pass features from

the encoder blocks to the corresponding decoder blocks. Each shortcut goes through a 3×3 convolutional layer (without altering channel size) to residues semantic gap [58]. Unlike UNet, element-wise summation is used to merge shortcut features and decoder features.

2) *Fabric representation module (FRM)*: The latent fabric representation module (FRM) (Figure 2 middle block) is located at the end of the second encoder residual block, and it is parameterised by hyper-parameters B and N :

- B is the number of branches (from $b = 1$ to $b = B$) in FRM. The input is tri-linear resized into B scales and processed processed through the B branches, respectively. The first branch $b = 1$ maintains all the dimensions of the input. As b increases from 1 to B , the spatial dimensions are progressively down-sampled by a factor of 2^{b-1} . In the meantime, the channel size progressively doubles also by a factor of 2^{b-1} to compensation for the loss of spatial resolution.
- N is the number of feature extractor nodes along each branch. The nodes are denoted $\psi_{n, b}$ (where $n \in \{1 \dots N\}$ and $b \in \{1 \dots B\}$) to indicate their locations in the FRM. To build a dense mesh of multi-scale sub-architectures, each node performs multi-scale feature extraction on outputs from its predecessor node (node input) and two neighbouring-branch predecessor nodes. That is, $\psi_{n, b}$ takes the outputs from $\psi_{n-1, b}$, $\psi_{n-1, b-1}$ and $\psi_{n-1, b+1}$ as inputs for processing.

3) *Fabric representation module node*: Each node (Figure 2 bottom block) consists of three components to perform multi-scale feature aggregation on the three inputs:

- Feature alignment (FA) module to resize the two neighbouring branch inputs (higher and lower resolution) to the size of the node input. First, two 3D convolutions are used to resize the channel dimension. Then, tri-linear up and down-sampling operations are used to resize the spatial dimensions.
- Trainable feature sum (TFS) module to combine the resized neighbouring inputs with the node input. Inspired by AutoDeepLab’s approach to architecture-level adaptability, here, we apply a trainable multiplicative weight to each input. Then, the intensity-scaled inputs are fused using element-wise summation. The three weights are normalised to between [0, 1] using the sigmoid function.
- Atrous Spatial Pyramid Pooling 3D (ASPP3D) module to perform multi-scale feature extraction on the fused inputs. Here, three parallel 3×3 dilated convolutions with rates 1, 2, and 4 are used. Combined with the multi-branch structure of FRM, ASPP3D increases the unique receptive field counts by a factor of 3, accounting for a large number of different scaled features. For example, an FRM with three branches each using ASPP3D nodes with dilation rates 1, 2 and 4 would yield nine unique receptive field sizes (3, 5, 6, 7, 10, 12, 14, 20 and 28). This would otherwise require nine dedicated branches without ASPP3D.

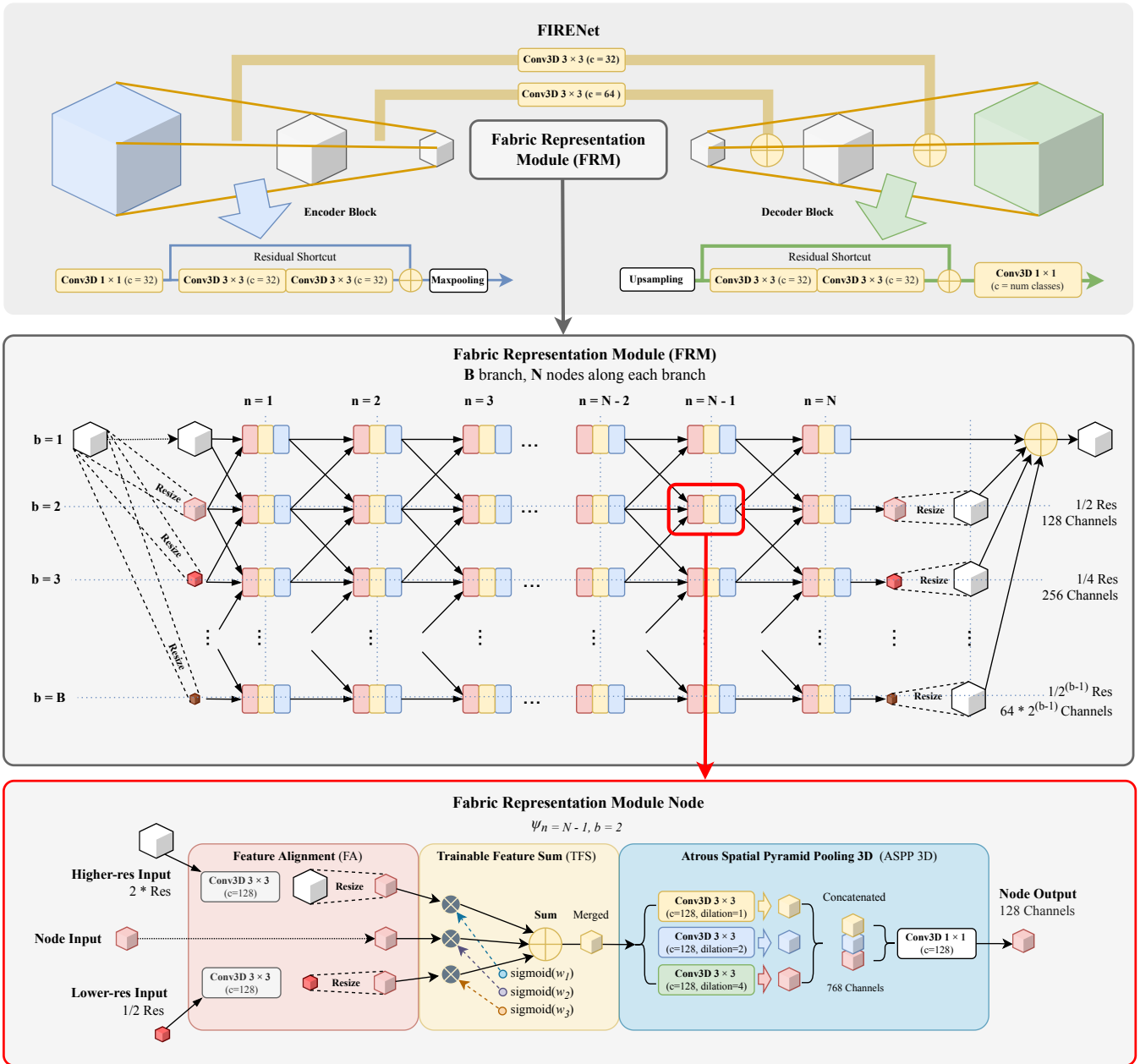


Fig. 2: Hierarchical component diagram of FIRENet including I) the high-level structure (top), II) the fabric representation module (FRM) (middle), and III) node structure diagram (bottom). FRM is designed to be diverse-scale and generalisable for multi-dataset processing. It contains B multi-scale branches and each branch has N nodes. The nodes are densely connected via trainable weights. The nodes perform further multi-scale feature extraction for a fine coverage of different feature sizes.

B. Multiple decoders for non-overlapping classes

Multiple decoders are used when training on datasets with few class overlaps. This is to reduce memory consumption since the segmentation channels cannot be sufficiently shared. As a workaround, each dataset is given a designated decoder, and only one decoder is active at a time. All the decoders are identical (to the decoder in Figure 2) except for the output channels. Although this workaround is a minor compromise for the otherwise entirely unified FIRENet, the majority of the diverse-scaled features are still shared via FRM.

C. Training

The loss function L_{seg} is a combination of the categorical cross-entropy loss and the Dice similarity coefficient (DSC) loss. The DSC loss was for each channel separately to avoid bias towards majority classes. FIRENet used deep supervision [30] during training as it has been shown to improve the performance of encoder-decoder segmentation models [26], [33]. The outputs from FRM and the intermediate decoder blocks are fed through a 1×1 3D convolution to produce auxiliary outputs. A separate segmentation loss

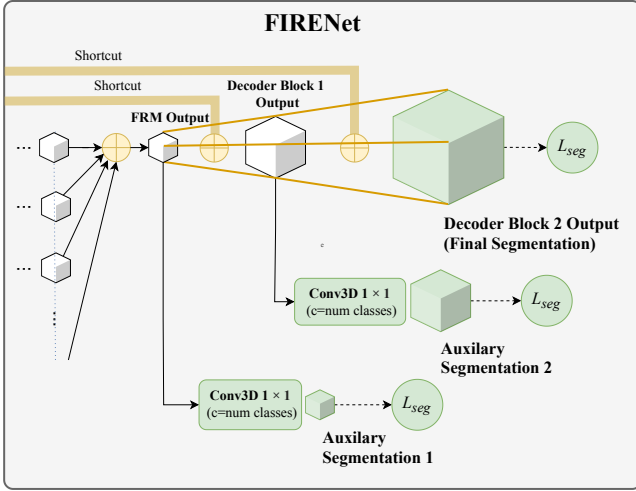


Fig. 3: FIRENet produces auxiliary segmentation outputs for deep supervision. There are two auxiliary outputs and one final output to compute the final loss.

L_{seg} is computed for auxiliary output and the total loss is the sum of all the segmentation losses.

The model was trained for 50 epochs using the Adam optimiser [27] and a batch size of 1. The hardware used for acceleration was an NVIDIA Tesla V100 (32GB) and the training lasted approximately 36 hours.

D. Experiment setups

The experiments involve applying FIRENet to multiple datasets with diverse image sizes. Since FIRENet can process non-uniform image sizes because of its emphasis on diverse-scale feature learning, there was no need to resize all the images to the same size (even for the extreme image sizes).

1) *Experiment I: Multi-dataset Transfer Learning:* FIRENet was tested for transfer learning involving several 3D medical imaging datasets. FIRENet was first pre-trained on a 3D prostate magnetic resonance (MR) dataset [15] (the prostate dataset). Then, the trained FIRENet was transferred for simultaneous multi-dataset bone segmentation on a composite bone dataset (the multi-bone dataset). Elastic deformation was used for data augmentation [41]. Consistent with the previous CAN3D work [11], 3-fold validation was used to split the prostate and the multi-bone dataset.

The prostate dataset contains 211 3D MR examinations of the pelvic region with manual segmentation labels for five foreground classes: body, bone (pelvic spine and girdle, proximal femur), urinary bladder, rectum and prostate. The multi-bone dataset is composed of four smaller datasets: three 3T MR imaging musculoskeletal (MSK) datasets (knee [20], shoulder [51], hip [4]) and the OAI knee [1] dataset. The main difficulty of segmenting the multi-bone dataset is the diverse image sizes and imbalanced numbers of training examples in each dataset (62, 25, 53 and 507 MR examinations, respectively). A 3-fold data split was applied to each constituent dataset. Smaller datasets were duplicated to ensure sample balance.

Due to the lack of existing simultaneous results for the multi-bone segmentation task, nnUNet was chosen and trained to establish a baseline. The preprocessing, training and evaluation stages were performed using the official code ¹. To ensure compatibility with the prescribed training pipeline, all the substituent bone datasets were pooled into a single dataset for binary bone segmentation.

2) *Experiment II: Simultaneous multi-dataset segmentation on MSD:* FIRENet was used to simultaneously segment the 10 datasets from the MSD model generalisability challenge. Most existing simultaneous multi-dataset segmentation works ([23] and [24]) were performed on a subset of these 10 datasets, excluding important and challenging tasks like HepaticVessel and Lung. The current work evaluated FIRENet on all 10 MSD datasets to provide a more thorough evaluation. These 10 datasets are highly diverse in image size and voxel spacing, with the smallest dimension being 11 voxels and the largest dimension being 751 voxels. For preprocessing, each image was re-sampled to the same voxel spacing of [1, 1, 1] (but not the same size) to retain the relative object sizes. Cropping was used sparingly only to cap large image dimensions to 180 voxels (which covers most of the image after re-sampling). Finally, voxel intensity standardisation was applied before entering the network. The dataset was divided into training and validation sets according to an 80%-20% split ratio as per previous work [33].

Since the 10 datasets have almost no class overlap, 10 decoders are used to produce segmentation maps for the 10 datasets, respectively. The training process iterates through the 10 datasets activating one decoder at a time (according to the dataset). The FRM, which contains learnt multi-scale features, was shared the whole time.

III. RESULTS AND DISCUSSION

A. Experiment I: Multi-dataset Transfer Learning

1) *FIRENet pre-training evaluation:* Table I shows the subject-level, 3-fold validation segmentation results from the prostate MR pre-training experiment for the body, bone, urinary bladder, rectum and prostate classes. FIRENet was compared to four other 3D deep learning baseline methods (3D UNet [8], improved UNet [26], VNet [37] and CAN3D [11]) on the same data splits. Overall FIRENet produced better results than these baseline methods in DSC, HD and mean surface distance values across multiple classes. In terms of the performance on outlier cases (min DSC), FIRENet was amongst the most resilient models producing less severe segmentation errors (indicated by the higher min DSCs in the table).

Table II shows results from published baseline methods [16], [3] on this prostate dataset. These results are presented separately as they are from statistical methods. Nonetheless, their quantitative results are comparable even to the more recent deep learning results (UNet and VNet), likely because deep learning requires a lot of training data. FIRENet and CAN3D were the only two methods significantly

¹<https://github.com/MIC-DKFZ/nnUNet>

TABLE I: Pre-training stage segmentation results of FIRENet on a MR prostate dataset compared against baseline methods 3D UNet, 3D improved UNet, VNet and CAN3D. The metrics listed are Dice similarity coefficient (DSC), Hausdorff distance (HD) and mean surface distance (MSD).

Class	Metrics	3D UNet [41]	3D improved UNet [26]	VNet [37]	CAN3D [11]	FIRENet
Body	DSC (mean \pm sd)	0.96 \pm 0.08	0.98 \pm 0.01	0.97 \pm 0.01	0.98 \pm 0.01	0.99 \pm 0.01
	HD (mean \pm sd)	42.73 \pm 37.42	35.80 \pm 12.02	29.00 \pm 9.34	30.57 \pm 11.36	13.08 \pm 6.48
	MSD (mean \pm sd)	3.61 \pm 7.78	1.03 \pm 0.69	1.33 \pm 0.55	0.95 \pm 0.61	0.47 \pm 0.38
	DSC (min)	0.65	0.91	0.92	0.92	0.93
Bone	DSC (mean \pm sd)	0.91 \pm 0.02	0.91 \pm 0.02	0.85 \pm 0.04	0.91 \pm 0.02	0.92 \pm 0.02
	HD (mean \pm sd)	36.35 \pm 23.70	41.05 \pm 28.78	51.33 \pm 17.70	39.73 \pm 24.48	13.19 \pm 11.09
	MSD (mean \pm sd)	1.65 \pm 0.42	1.52 \pm 0.39	2.54 \pm 1.15	1.50 \pm 0.38	0.85 \pm 0.22
	DSC (min)	0.80	0.85	0.67	0.84	0.85
Bladder	DSC (mean \pm sd)	0.87 \pm 0.21	0.93 \pm 0.10	0.80 \pm 0.16	0.92 \pm 0.13	0.93 \pm 0.10
	HD (mean \pm sd)	30.53 \pm 40.06	27.94 \pm 35.66	39.61 \pm 36.36	33.89 \pm 37.92	9.50 \pm 16.49
	MSD (mean \pm sd)	4.53 \pm 12.69	2.10 \pm 3.99	3.91 \pm 3.01	2.51 \pm 5.44	1.35 \pm 3.37
	DSC (min)	0.00	0.27	0.07	0.06	0.23
Rectum	DSC (mean \pm sd)	0.78 \pm 0.11	0.87 \pm 0.05	0.76 \pm 0.09	0.85 \pm 0.05	0.87 \pm 0.05
	HD (mean \pm sd)	27.74 \pm 28.71	18.53 \pm 25.34	38.28 \pm 45.40	33.30 \pm 36.65	14.14 \pm 20.76
	MSD (mean \pm sd)	3.16 \pm 2.93	1.71 \pm 1.10	3.62 \pm 5.95	2.08 \pm 1.45	1.24 \pm 1.29
	DSC (min)	0.18	0.67	0.29	0.66	0.64
Prostate	DSC (mean \pm sd)	0.75 \pm 0.18	0.84 \pm 0.08	0.74 \pm 0.13	0.81 \pm 0.10	0.86 \pm 0.06
	HD (mean \pm sd)	28.23 \pm 69.67	8.91 \pm 9.17	25.38 \pm 29.83	14.28 \pm 16.33	7.36 \pm 10.10
	MSD (mean \pm sd)	15.85 \pm 65.41	1.92 \pm 0.87	3.54 \pm 2.89	2.17 \pm 0.99	1.13 \pm 0.48
	DSC (min)	0.00	0.45	0.08	0.39	0.51

TABLE II: Pre-training stage segmentation results of FIRENet on a MR prostate dataset compared with published traditional baselines. FIRENet used 3-fold validation and the traditional methods used leave-one-out. The metrics listed are Dice similarity coefficient (DSC), Hausdorff distance (HD) and mean surface distance (MSD).

Method	Median Body DSC	Median Bone DSC	Median Bladder DSC	Median Rectum DSC	Median Prostate DSC	Median Prostate MSD (mm)	Median Prostate HD (mm)	Mean Prostate DSC
Dowling et al.[16]	1	0.92	0.86	0.85	0.82	2.04	13.3	0.80
Chandra et al.[3]	0.94	0.81	0.87	0.79	0.81	2.08	9.60	0.79
FIRENet	0.99	0.92	0.96	0.89	0.87	1.00	4.24	0.86

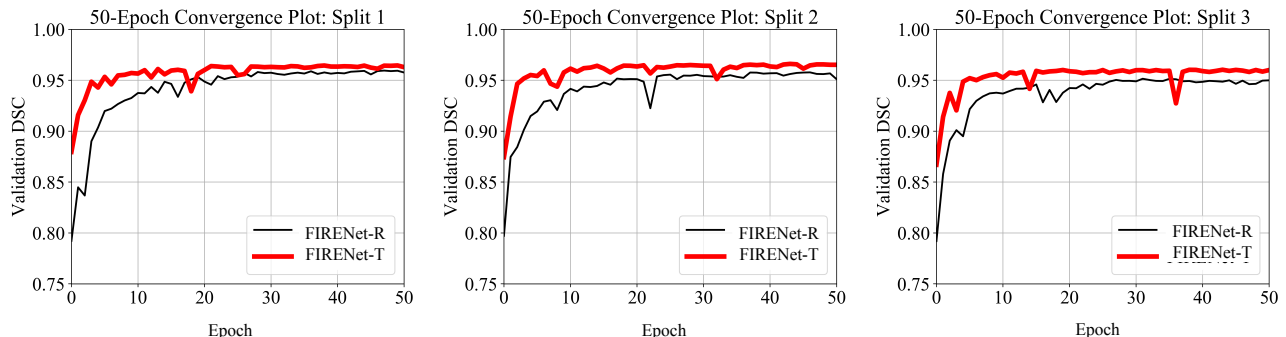


Fig. 4: Convergence plots comparing FIRENet-R (randomly initialised) and FIRENet-T (pre-trained on the prostate dataset and fine-tuned on the four MSK bone datasets). The DSCs for the bones were averaged across the multi-bone dataset. FIRENet-T consistently showed accelerated convergence, especially in the first 30 epochs.

exceeding these non-deep-learning methods, especially across the most challenging classes (prostate and rectum).

2) *Transfer learning*: For the transfer learning part of the experiment, two FIRENet instances were trained on the multi-bone dataset: a FIRENet with weights pre-trained on the prostate dataset (FIRENet-T) and a randomly initialised FIRENet (FIRENet-R). The multi-bone segmentation results of FIRENet-R and FIRENet-T are compared in Tables III and Figure 6. Overall, both FIRENet-R and T exhibited the ability to simultaneously segment diverse medical image data despite relying on only one shared set of weights: their results on the OAI dataset are comparable to other methods [11], [1] which published results optimised for only one dataset. Comparing

the mean DSC values of FIRENet-R and FIRENet-T, it can be seen that FIRENet-T could leverage pre-training to improve the segmentation performance across all the constituent bone datasets. Moreover, as Figure 6 shows, FIRENet-T’s lowest DSC results were also noticeably improved over FIRENet-R, indicating reduced critical segmentation errors. In terms of convergence, FIRENet-T was also more stable and faster (Figure 4) supporting the benefits of transfer learning for simultaneous multi-dataset segmentation.

nnUNet was chosen and trained to establish a baseline for the multi-bone segmentation experiment. However, unlike FIRENet, the multi-bone segmentation results from nnUNet indicate that it is less suitable for simultaneous multi-dataset

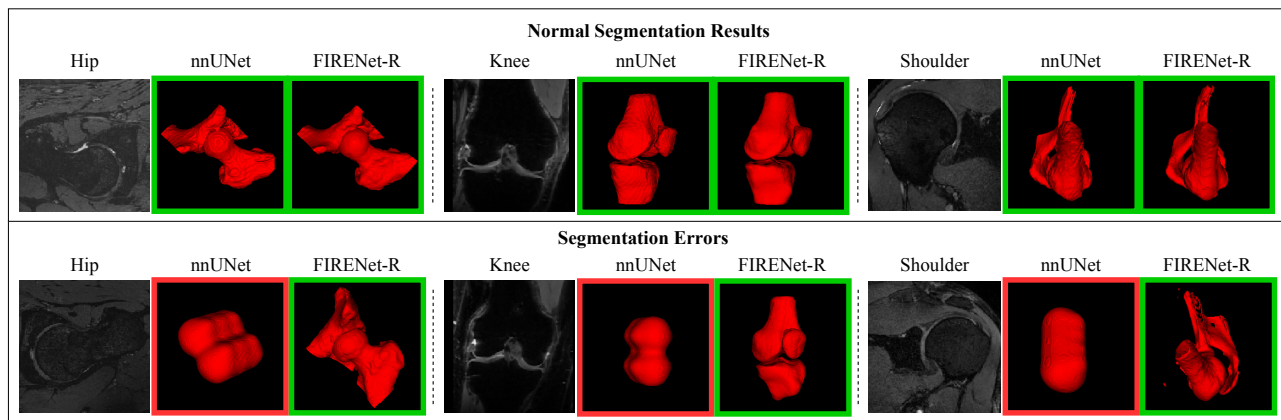


Fig. 5: Comparison of FIRENet and nnUNet when handling multiple datasets with diverse image sizes. FIRENet appeared more resilient, producing valid results in all three cases (and also for the entire dataset) and nnUNet appeared to have struggled to be consistent. Both methods used the same data splits, and nnUNet was built and trained using the official nnUNet scripts.

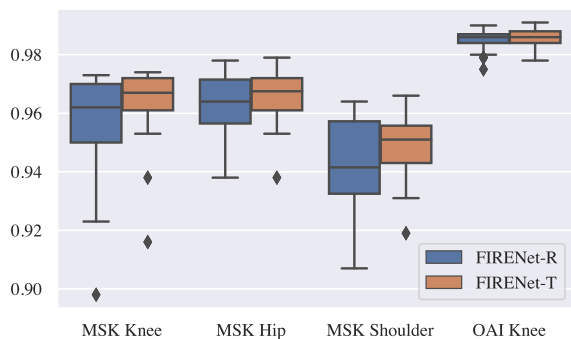


Fig. 6: Box plot comparing FIRENet-R and FIRENet-T results on the multi-bone dataset. The corresponding quantitative results can be found in Table III.

processing - the best nnUNet DSCs were substantially lower at 0.612, 0.851, 0.633 and 0.986 for the MSK hip, knee, shoulder and OAI, respectively. In this case, nnUNet produce inconsistent segmentation result. As the segmentation visualisation in Figure 5 shows, there were unpredictable failures in nnUNet’s results on three of the four constituent datasets (MSK knee, shoulder and hip). It was also observed that the training process of nnUNet was highly unstable, and early stopping was required to obtain some usable results (which were already presented in this section). nnUNet’s inability to produce consistent and satisfactory results could be attributed to its one-size-fits-all self-configuring procedure, as well as the lack of rich-scale feature extraction as desired by multi-dataset applications. On the contrary, FIRENet-R and FIRENet-T were designed to be voided of dataset-specific configurations, there is also a strong emphasis on multi-dataset feature learning to cover different data sizes.

TABLE III: Mean bone segmentation Dice similarity coefficients (DSCs) of FIRENet-R (randomly initialised) and FIRENet-T (pre-trained on a prostate dataset and fine-tuned on the four MSK bone datasets) compared to other baseline methods. nnUNet was trained by treating all four bone datasets as one. FIRENet appeared more adaptable when applied to multiple datasets with non-uniform image sizes. Whereas nnUNet was prone to segmentation failure (see examples in Figure 5). The cited previous methods only applied to and reported single-dataset results.

Method	Hip	Knee	Shoulder	OAI	Overall
FIRENet-R	0.954	0.961	0.940	0.985	0.952
FIRENet-T	0.962	0.965	0.947	0.986	0.965
nnUNet	0.612	0.851	0.633	0.986	-
CAN3D [11]	-	-	-	0.986	-
SSM+CNN [1]	-	-	-	0.985	-
SSM [4]	0.950	-	-	-	-
SSM [20]	-	0.922	-	-	-
SSM [51]	-	-	0.8815	-	-

B. Experiment II: Simultaneous multi-dataset segmentation on Medical Segmentation Decathlon (MSD)

In this experiment, FIRENet’s segmentation performance was compared to the recently published simultaneous multi-dataset segmentation methods (3D MDUNet [33] and 3D U²Net), and some example predictions are visualised in Figure 7. As IV shows, compared to 3D MDUNet and its 3D U²Net baseline (as reported in the 3D MDUNet publication), FIRENet’s DSC results in the Hippocampus, Pancreas and Spleen segmentation tasks are considerably improved. Compared to the original 3D U²Net, FIRENet achieved significantly better Pancreas segmentation DSC (by 12.1%), and similar segmentation DSCs in the Heart, Liver and Prostate segmentation tasks. However, it did also underperform in terms of Hippocampus segmentation DSC. It is worth noting that both the 3D MDUNet and 3D U²Net only involved a subset of the MSD challenge and, by extension, only a subset of the challenge’s complexity. In the meantime,

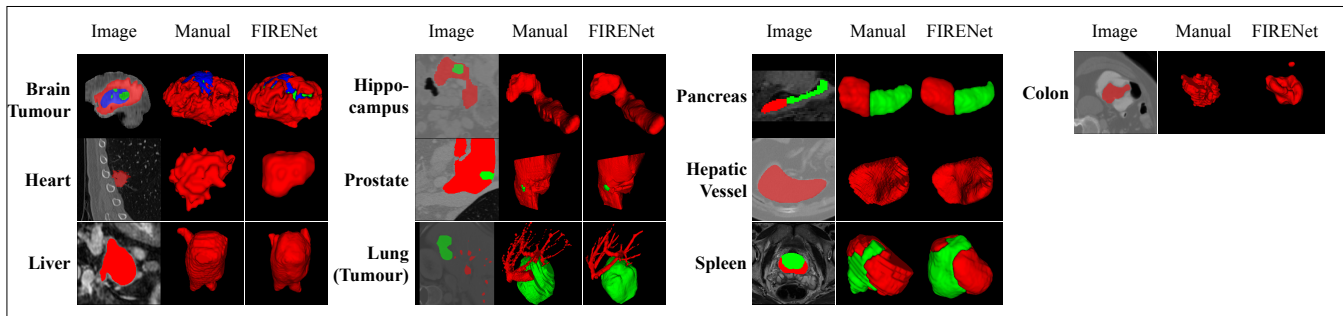


Fig. 7: FIRENet’s simultaneous segmentation results on the 10 MSD datasets. The image dimensions are highly diverse in size with a difference of up to 4 times for each dimension.

TABLE IV: FIRENet’s simultaneous segmentation DSC results on the full MSD dataset. The baseline methods for comparison are 3D MDUNet [33] and 3D U²Net. All of the DSC results were computed without the background class.

Task Code	FIRENet	3D MDUNet	3D MDUNet(3D U ² Net baseline)	3D U ² Net(universal)
Task01_BrainTumour	0.571	-	-	-
Task02_Heart	0.913	0.921	0.913	0.919
Task03_Liver	0.917	-	-	0.935
Task04_Hippocampus	0.826	0.650	0.624	0.882
Task05_Prostate	0.807	-	-	0.789
Task06_Lung	0.778	-	-	-
Task07_Pancreas	0.742	0.622	0.534	0.621
Task08_HepaticVessel	0.787	-	-	-
Task09_Spleen	0.895	0.833	0.815	-
Task10_Colon	0.437	-	-	-

FIRENet was trained on all 10 datasets.

While nnUNet has been the gold standard in the MSD challenge, as experiment I shows, pooling different datasets together is not within the scope of nnUNet’s design. Although nnUNet’s results on individual acMSD datasets have been state-of-the-art, they were all specially tuned for one dataset at a time. Hence, nnUNet’s single dataset results were not included in the performance comparison with other methods for this experiment.

C. Architecture-level generalisability

FIRENet exhibited excellent architecture-level generalisability as it can seamlessly transfer between and apply to multiple datasets. The two experiments reported cover applications in various scenarios including single dataset learning, transfer learning and simultaneous multi-dataset learning. Despite the significant differences in image sizes, object appearances and number of samples, No hyper-parameter modification was required between experiments showing the benefits of an all-inclusive fabric architecture. The only workaround required was the use of multiple decoders to save memory (in the MSD segmentation experiment).

D. Limitations

As FIRENet universally applies to different imaging datasets, its design and training methodology purposefully lack domain-specific optimisations. Compared to public challenge results produced by highly specialised and single-dataset methods, a general architecture does not often yield optimal numerical results across all the different datasets. Although FIRENet’s architecture is free of overhead in

handling multiple datasets, there is an increase in total model size with each additional decoder (required for different output formats). Finally, as a CNN, FIRENet faces the current limitations of deep learning. For example, the lack of clinical explain-ability and difficulty extrapolating to unseen data distributions.

E. Future work

As new labelled medical imaging datasets and deep learning accelerators become available, FIRENet’s size and training set composition can continue to expand. It also would be beneficial to train multiple instances of FIRENet to specialise in different imaging modalities or anatomical structures. In terms of architectural development, FIRENet could be effectively re-purposed for classification, regression and multi-task learning by adding downstream prediction heads. For example, a classification head could be attached to the output of FRM for 3D medical image classification based on the features extracted.

IV. CONCLUSION

To better take advantage of the scattered dataset in medical image analysis, this work presents FIRENet, a versatile 3D neural network architecture geared towards simultaneous multi-dataset learning and segmentation. In the prostate, multi-bone and MSD segmentation experiments, FIRENet exhibited superior multi-dataset adaptability without dataset specific tuning or even hyper-parameter modification. In contrast, existing works in the literature either performed poorly across multiple datasets or were limited to a small number of datasets. The technical contribution of FIRENet is the multi-scale

fabric representation module (FRM), which acts as a superposition of many possible sub-architectures alleviating the need for dataset-specific architecture design. In addition, node in FRM employs ASPP 3D for further diverse-scale feature extraction, which ensures fine-grained coverage of different scaled features. For future work, FIRENet’s FRM has the potential to serve as a backbone feature extractor for other 3D medical image analysis tasks.

REFERENCES

- [1] Felix Ambellan, Alexander Tack, Moritz Ehlke, and Stefan Zachow. Automated segmentation of knee bone and cartilage combining statistical shape knowledge and convolutional neural networks: Data from the osteoarthritis initiative. *Medical Image Analysis*, 52:109 – 118, 2019.
- [2] Pierre Buysse, Abderrahim Elmoataz, and Olivier Lezoray. Multiscale convolutional neural networks for vision-based classification of cells. volume 7725, 11 2012.
- [3] Shekhar S Chandra, Jason A Dowling, Peter B Greer, Jarad Martin, Chris Wratten, Peter Pichler, Jurgen Fripp, and Stuart Crozier. Fast automated segmentation of multiple objects via spatially weighted shape learning. *Physics in Medicine and Biology*, 61(22):8070–8084, oct 2016.
- [4] Shekhar S. Chandra, Ying Xia, Craig Engstrom, Stuart Crozier, Raphael Schwarz, and Jurgen Fripp. Focused shape models for hip joint segmentation in 3D magnetic resonance images. *Medical Image Analysis*, 18(3):567 – 578, 2014.
- [5] Liang-Chieh Chen, George Papandreou, Florian Schroff, and Hartwig Adam. Rethinking Atrous Convolution for Semantic Image Segmentation. *arXiv e-prints*, page arXiv:1706.05587, June 2017.
- [6] Liang-Chieh Chen, Yukun Zhu, George Papandreou, Florian Schroff, and Hartwig Adam. Encoder-decoder with atrous separable convolution for semantic image segmentation. In Vittorio Ferrari, Martial Hebert, Cristian Sminchisescu, and Yair Weiss, editors, *Computer Vision – ECCV 2018*, pages 833–851, Cham, 2018. Springer International Publishing.
- [7] Sihong Chen, Kai Ma, and Yefeng Zheng. Med3D: Transfer Learning for 3D Medical Image Analysis. *arXiv e-prints*, page arXiv:1904.00625, April 2019.
- [8] Özgün Çiçek, Ahmed Abdulkadir, Soeren S. Lienkamp, Thomas Brox, and Olaf Ronneberger. 3D U-Net: Learning dense volumetric segmentation from sparse annotation. In Sebastian Ourselin, Leo Joskowicz, Mert R. Sabuncu, Gozde Unal, and William Wells, editors, *Medical Image Computing and Computer-Assisted Intervention – MICCAI 2016*, pages 424–432, Cham, 2016. Springer International Publishing.
- [9] Marius Cordts, Mohamed Omran, Sebastian Ramos, Timo Rehfeld, Markus Enzweiler, Rodrigo Benenson, Uwe Franke, Stefan Roth, and Bernt Schiele. The cityscapes dataset for semantic urban scene understanding. In *Proceedings of the IEEE Conference on Computer Vision and Pattern Recognition (CVPR)*, June 2016.
- [10] Z. Cui, J. Yang, and Y. Qiao. Brain MRI segmentation with patch-based CNN approach. In *2016 35th Chinese Control Conference (CCC)*, pages 7026–7031, 2016.
- [11] Wei Dai, Boyeong Woo, Siyu Liu, Matthew Marques, Craig Engstrom, Peter B. Greer, Stuart Crozier, Jason A. Dowling, and Shekhar S. Chandra. CAN3D: Fast 3D medical image segmentation via compact context aggregation. *Medical Image Analysis*, 82:102562, November 2022.
- [12] Jose Dolz, Christian Desrosiers, and Ismail Ben Ayed. 3D fully convolutional networks for subcortical segmentation in MRI: A large-scale study. *NeuroImage*, 170:456 – 470, 2018.
- [13] Suyu Dong, Gongning Luo, Clara Tam, Wei Wang, Kuanquan Wang, Shaodong Cao, Bo Chen, Henggui Zhang, and Shuo Li. Deep atlas network for efficient 3D left ventricle segmentation on echocardiography. *Medical Image Analysis*, 61:101638, 2020.
- [14] Qi Dou, Lequan Yu, Hao Chen, Yueming Jin, Xin Yang, Jing Qin, and Pheng-Ann Heng. 3D deeply supervised network for automated segmentation of volumetric medical images. *Medical Image Analysis*, 41:40 – 54, 2017. Special Issue on the 2016 Conference on Medical Image Computing and Computer Assisted Intervention (Analog to MICCAI 2015).
- [15] Jason Dowling and Peter Greer. Labelled weekly MR images of the male pelvis, 2021.
- [16] Jason A. Dowling, Jidi Sun, Peter Pichler, David Rivest-Hénault, Soumya Ghose, Haylea Richardson, Chris Wratten, Jarad Martin, Jameen Arm, Leah Best, Shekhar S. Chandra, Jurgen Fripp, Frederick W. Menk, and Peter B. Greer. Automatic substitute computed tomography generation and contouring for magnetic resonance imaging (MRI)-alone external beam radiation therapy from standard MRI sequences. *International Journal of Radiation Oncology*Biophysics*, 93(5):1144 – 1153, 2015.
- [17] David Eigen and Rob Fergus. Predicting depth, surface normals and semantic labels with a common multi-scale convolutional architecture. pages 2650–2658, 2015.
- [18] M. Everingham, L. Van Gool, C. K. I. Williams, J. Winn, and A. Zisserman. The Pascal Visual Object Classes (VOC) Challenge. *International Journal of Computer Vision*, 88(2):303–338, June 2010.
- [19] Damien Fourrere, Rémi Emonet, Elisa Fromont, Damien Muselet, Alain Tremeau, and Christian Wolf. Residual Conv-Deconv Grid Network for Semantic Segmentation. *arXiv e-prints*, page arXiv:1707.07958, July 2017.
- [20] Jurgen Fripp, Stuart Crozier, Simon K Warfield, and Sébastien Ourselin. Automatic segmentation of the bone and extraction of the bone–cartilage interface from magnetic resonance images of the knee. *Physics in Medicine and Biology*, 52(6):1617–1631, feb 2007.
- [21] Ali Hatamizadeh, Yucheng Tang, Vishwesh Nath, Dong Yang, Andriy Myronenko, Bennett Landman, Holger R. Roth, and Daguang Xu. Unetr: Transformers for 3D medical image segmentation. In *Proceedings of the IEEE/CVF Winter Conference on Applications of Computer Vision (WACV)*, pages 574–584, January 2022.
- [22] Kaiming He, Xiangyu Zhang, Shaoqing Ren, and Jian Sun. Deep Residual Learning for Image Recognition. In *Proceedings of the IEEE Conference on Computer Vision and Pattern Recognition (CVPR)*, pages 770–778, 06 2016.
- [23] Chao Huang, Hu Han, Qingsong Yao, Shankuan Zhu, and S. Kevin Zhou. 3d u²-net: A 3D universal u-net for multi-domain medical image segmentation. In *Lecture Notes in Computer Science*, pages 291–299. Springer International Publishing, 2019.
- [24] Rui Huang, Yuanjie Zheng, Zhiqiang Hu, Shaoting Zhang, and Hongsheng Li. Multi-organ segmentation via co-training weight-averaged models from few-organ datasets. In *Medical Image Computing and Computer Assisted Intervention – MICCAI 2020*, pages 146–155. Springer International Publishing, 2020.
- [25] Fabian Isensee, Paul F. Jaeger, Simon A. A. Kohl, Jens Petersen, and Klaus H. Maier-Hein. nnU-net: a self-configuring method for deep learning-based biomedical image segmentation. *Nature Methods*, 18(2):203–211, December 2020.
- [26] Fabian Isensee, Philipp Kickingereder, Wolfgang Wick, Martin Bendzus, and Klaus Maier-Hein. Brain Tumor Segmentation and Radiomics Survival Prediction: Contribution to the BRATS 2017 Challenge, pages 287–297. 09 2018.
- [27] Diederik Kingma and Jimmy Ba. Adam: A method for stochastic optimization. *International Conference on Learning Representations*, 12 2014.
- [28] F. Knoll, K. Hammernik, E. Kobler, T. Pock, M. P. Recht, and D. K. Sodickson. Assessment of the generalization of learned image reconstruction and the potential for transfer learning. *Magn Reson Med*, 81(1):116–128, 2019.
- [29] Alex Krizhevsky, Ilya Sutskever, and Geoffrey E Hinton. ImageNet Classification with Deep Convolutional Neural Networks. In F. Pereira, C. J. C. Burges, L. Bottou, and K. Q. Weinberger, editors, *Proceedings of the International Conference on Neural Information Processing Systems (NIPS)*, volume 25. Curran Associates, Inc., 2012.
- [30] Chen-Yu Lee, Saining Xie, Patrick Gallagher, Zhengyou Zhang, and Zhuowen Tu. Deeply-Supervised Nets. In Guy Lebanon and S. V. N. Vishwanathan, editors, *Proceedings of the Eighteenth International Conference on Artificial Intelligence and Statistics*, volume 38 of *Proceedings of Machine Learning Research*, pages 562–570, San Diego, California, USA, 09–12 May 2015. PMLR.
- [31] S. Li, X. Zhu, and J. Bao. Hierarchical Multi-Scale Convolutional Neural Networks for Hyperspectral Image Classification. *Sensors (Basel)*, 19(7), Apr 2019.
- [32] Ailiang Lin, Bingzhi Chen, Jiayu Xu, Zheng Zhang, Guangming Lu, and David Zhang. DS-TransUNet: Dual swin transformer u-net for medical image segmentation. *IEEE Transactions on Instrumentation and Measurement*, 71:1–15, 2022.

- [33] Manying Lin, Qingling Cai, and Jun Zhou. 3D Md-Unet: A novel model of multi-dataset collaboration for medical image segmentation. *Neurocomputing*, 492:530–544, July 2022.
- [34] Tsung-Yi Lin, Michael Maire, Serge Belongie, James Hays, Pietro Perona, Deva Ramanan, Piotr Dollár, and C. Lawrence Zitnick. Microsoft coco: Common objects in context. In David Fleet, Tomas Pajdla, Bernt Schiele, and Tinne Tuytelaars, editors, *Computer Vision – ECCV 2014*, pages 740–755, Cham, 2014. Springer International Publishing.
- [35] Chenxi Liu, Liang-Chieh Chen, Florian Schroff, Hartwig Adam, Wei Hua, Alan Yuille, and Li Fei-Fei. Auto-deeplab: Hierarchical neural architecture search for semantic image segmentation. In *Proceedings of the IEEE Conference on Computer Vision and Pattern Recognition (CVPR)*, pages 82–92, 06 2019.
- [36] I. Y. Maolood, Y. E. A. Al-Salhi, and S. Lu. Thresholding for Medical Image Segmentation for Cancer using Fuzzy Entropy with Level Set Algorithm. *Open Med (Wars)*, 13:374–383, 2018.
- [37] Fausto Milletari, Nassir Navab, and Seyed-Ahmad Ahmadi. V-Net: Fully Convolutional Neural Networks for Volumetric Medical Image Segmentation. In *2016 Fourth International Conference on 3D Vision (3DV)*, pages 565–571, 2016.
- [38] Hafiz Tayyab Mustafa, Jie Yang, and Masoumeh Zareapoor. Multi-scale convolutional neural network for multi-focus image fusion. *Image and Vision Computing*, 85:26 – 35, 2019.
- [39] Zhen-Liang Ni, Gui-Bin Bian, Xiao-Hu Zhou, Zeng-Guang Hou, Xiao-Liang Xie, Chen Wang, Yan-Jie Zhou, Rui-Qi Li, and Zhen Li. RAUNet: Residual Attention U-Net for Semantic Segmentation of Cataract Surgical Instruments. *arXiv e-prints*, page arXiv:1909.10360, September 2019.
- [40] Hariharan Ravishankar, Prasad Sudhakar, Rahul Venkataramani, Shehadri Thiruvankadam, Pavan Annangi, Narayanan Babu, and Vivek Vaidya. Understanding the mechanisms of deep transfer learning for medical images. In Gustavo Carneiro, Diana Mateus, Loïc Peter, Andrew Bradley, João Manuel R. S. Tavares, Vasileios Belagiannis, João Paulo Papa, Jacinto C. Nascimento, Marco Loog, Zhi Lu, Jaime S. Cardoso, and Julien Cornébis, editors, *Deep Learning and Data Labeling for Medical Applications*, pages 188–196, Cham, 2016. Springer International Publishing.
- [41] Olaf Ronneberger, Philipp Fischer, and Thomas Brox. U-net: Convolutional networks for biomedical image segmentation. In Nassir Navab, Joachim Hornegger, William M. Wells, and Alejandro F. Frangi, editors, *Medical Image Computing and Computer-Assisted Intervention – MICCAI 2015*, pages 234–241, Cham, 2015. Springer International Publishing.
- [42] Shreyas Saxena and Jakob Verbeek. Convolutional neural fabrics. In *Proceedings of the International Conference on Neural Information Processing Systems (NIPS)*, NIPS’16, page 4060–4068, Red Hook, NY, USA, 2016. Curran Associates Inc.
- [43] G. Sharp, K. D. Fritscher, V. Pekar, M. Peroni, N. Shusharina, H. Veeraraghavan, and J. Yang. Vision 20/20: perspectives on automated image segmentation for radiotherapy. *Med Phys*, 41(5):050902, May 2014.
- [44] H. C. Shin, H. R. Roth, M. Gao, L. Lu, Z. Xu, I. Nogues, J. Yao, D. Mollura, and R. M. Summers. Deep Convolutional Neural Networks for Computer-Aided Detection: CNN Architectures, Dataset Characteristics and Transfer Learning. *IEEE Trans Med Imaging*, 35(5):1285–1298, 05 2016.
- [45] Karen Simonyan and Andrew Zisserman. Very Deep Convolutional Networks for Large-Scale Image Recognition. *arXiv e-prints*, page arXiv:1409.1556, September 2014.
- [46] Liyan Sun, Wenao Ma, Xinghao Ding, Yue Huang, Dong Liang, and John Paisley. A 3D spatially weighted network for segmentation of brain tissue from MRI. *IEEE Transactions on Medical Imaging*, 39(4):898–909, April 2020.
- [47] Jeya Maria Jose Valanarasu, Vishwanath A. Sindagi, Ilker Hacihaliloglu, and Vishal M. Patel. KiU-net: Overcomplete convolutional architectures for biomedical image and volumetric segmentation. *IEEE Transactions on Medical Imaging*, 41(4):965–976, April 2022.
- [48] Jingdong Wang, Ke Sun, Tianheng Cheng, Borui Jiang, Chaorui Deng, Yang Zhao, Dong Liu, Yadong Mu, Mingkui Tan, Xinggang Wang, Wenyu Liu, and Bin Xiao. Deep high-resolution representation learning for visual recognition. *IEEE Transactions on Pattern Analysis and Machine Intelligence*, pages 1–1, 2020.
- [49] Samir S. Yadav and Shivajirao M. Jadhav. Deep convolutional neural network based medical image classification for disease diagnosis. *Journal of Big Data*, 6(1):113, Dec 2019.
- [50] Ke Yan, Jinzheng Cai, Youjing Zheng, Adam P. Harrison, Dakai Jin, Youbao Tang, Yuxing Tang, Lingyun Huang, Jing Xiao, and Le Lu. Learning from multiple datasets with heterogeneous and partial labels for universal lesion detection in CT. *IEEE Transactions on Medical Imaging*, 40(10):2759–2770, October 2021.
- [51] Zhengyi Yang, Jurgen Fripp, Shekhar S Chandra, AleÅ; Neubert, Ying Xia, Mark Strudwick, Anthony Paproki, Craig Engstrom, and Stuart Crozier. Automatic bone segmentation and bone-cartilage interface extraction for the shoulder joint from magnetic resonance images. *Physics in Medicine and Biology*, 60(4):1441, 2015.
- [52] Jason Yosinski, Jeff Clune, Yoshua Bengio, and Hod Lipson. How transferable are features in deep neural networks? *Proceedings of the International Conference on Neural Information Processing Systems (NIPS)*, 27:3320–3328, 2014.
- [53] F. Yu and V. Koltun. Multi-scale context aggregation by dilated convolutions. *CoRR*, abs/1511.07122, 2016.
- [54] Qihang Yu, Dong Yang, Holger Roth, Yutong Bai, Yixiao Zhang, Alan L. Yuille, and Daguang Xu. C2fnas: Coarse-to-fine neural architecture search for 3D medical image segmentation. In *Proceedings of the IEEE Conference on Computer Vision and Pattern Recognition (CVPR)*. IEEE, June 2020.
- [55] Zhengxin Zhang, Qingjie Liu, and Yunhong Wang. Road Extraction by Deep Residual U-Net. *IEEE Geoscience and Remote Sensing Letters*, 15(5):749–753, May 2018.
- [56] Hengshuang Zhao, Jianping Shi, Xiaojuan Qi, Xiaogang Wang, and Jiaya Jia. Pyramid scene parsing network. In *Proceedings of the IEEE Conference on Computer Vision and Pattern Recognition (CVPR)*, pages 6230–6239, 2017.
- [57] Yisu Zhou, Xiaolin Hu, and Bo Zhang. Interlinked convolutional neural networks for face parsing. volume 9377, pages 222–231, 10 2015.
- [58] Zongwei Zhou, Md Mahfuzur Rahman Siddiquee, Nima Tajbakhsh, and Jianming Liang. Unet++: A nested u-net architecture for medical image segmentation. In Danail Stoyanov, Zeike Taylor, Gustavo Carneiro, Tanveer Syeda-Mahmood, Anne Martel, Lena Maier-Hein, João Manuel R.S. Tavares, Andrew Bradley, João Paulo Papa, Vasileios Belagiannis, Jacinto C. Nascimento, Zhi Lu, Sailesh Conjeti, Mehdi Moradi, Hayit Greenspan, and Anant Madabhushi, editors, *Deep Learning in Medical Image Analysis and Multimodal Learning for Clinical Decision Support*, pages 3–11, Cham, 2018. Springer International Publishing.
- [59] Hancan Zhu, Feng Shi, Li Wang, Sheng-Che Hung, Meng-Hsiang Chen, Shuai Wang, Weili Lin, and Dinggang Shen. Dilated dense u-net for infant hippocampus subfield segmentation. *Frontiers in Neuroinformatics*, 13:30, 2019.
- [60] Barret Zoph and Quoc V. Le. Neural architecture search with reinforcement learning. 2017.